ICES REPORT 17-12

June 2017

Adaptive Numerical Homogenization for Upscaling Single Phase Flow and Transport

by

Yerlan Amanbek, Gurpreet Singh, Mary F. Wheeler, and Hans van Duijn

The Institute for Computational Engineering and Sciences
The University of Texas at Austin
Austin, Texas 78712

Reference: Yerlan Amanbek, Gurpreet Singh, Mary F. Wheeler, and Hans van Duijn, "Adaptive Numerical Homogenization for Upscaling Single Phase Flow and Transport," ICES REPORT 17-12, The Institute for Computational Engineering and Sciences, The University of Texas at Austin, June 2017.

Adaptive Numerical Homogenization for Upscaling Single Phase Flow and Transport

Yerlan Amanbek* Gurpreet Singh Mary F. Wheeler Hans van Duijn

June 13, 2017

Abstract

We propose an adaptive multiscale approach to improve the efficiency and the accuracy of numerical computations by combining upscaling and domain decomposition methods. The key objective of this work is to develop upscaling approaches to minimize the use of fine scale information for time varying initial and boundary conditions. This includes changes in well parameter such as injection composition and specifications as well as in situ or initial conditions. A fine scale flow and transport problem is solved only in specific subdomains while solving a coarse scale problem in the rest of the domain. This involves special treatment of sharp interfaces associated with the transport equations. We define transient regions as subdomains where spatial changes in concentration are significant. Away from the transient regions, upscaling is performed locally by using a numerical homogenization to obtain effective equations at the macroscopic scale. A fine grid is then used in the transient regions and a coarse grid everywhere else resulting in a non-matching multi-block problem. We use the Enhanced Velocity Mixed Finite Element Method (EVMFEM) as a domain decomposition approach to couple the coarse and fine subdomains [42]. To the authors' knowledge, this integrated approach has not been investigated either theoretically or computationally in the existing literature. A number of numerical tests are also presented for verifying and demonstrating the capability of the adaptive numerical homogenization approach in upscaling flow and transport in porous medium.

Keywords. enhanced velocity, numerical homogenization, adaptive mesh refinement, multiscale methods

1 Introduction

Accurate modeling of flow and transport in subsurface is important in petroleum reservoir recovery evaluations, nuclear waste disposal systems, CO_2 sequestration, and groundwater remediation. Efficient numerical modeling of the associated physical processes has several challenges due to heterogeneity, uncertainty and multiscale nature of the porous media parameters. The main source these parameters are usually borehole measurements which are sparsely distributed spatially. The reservoir parameters are populated using these measurements in conjunction with geostatistical methods including parameter estimation and uncertainty quantification. However, a direction numerical simulation of the flow and transport problem, for a given scenario, using these fine scale parameters is computationally prohibitive. Additionally, the data sets obtained from different observation methods vary strongly in characteristic spatial scales. For example, borehole and seismic measurements

have a resolution varying between a few feet to hundreds of feet, respectively. A coarse scale numerical model, which can handle multiple Representative Elementary Volumes (REV), is therefore necessary to reduce computational overheads associated with solving a fine scale problem. However, ad-hoc averaging techniques might fail to capture fine scale features resulting in loss of solution accuracy compromising the predictive nature of the model. Thus, development of mathematically consistent upscaling techniques is equally necessary for preserving solution accuracy at macroscopic scales. The multiscale nature of the flow and transport problems in porous medium has been addressed by several others [24, 8, 7, 10, 21, 44] giving rise to a number of approaches for upscaling. Each of these approaches perform computations at a coarse scale aiming to capture fine scale physics as closely as possible. However, one must note that all upscaling approaches tend to average fine scale features to obtain coarse scale solution resulting in an acceptable loss of accuracy. In what follows, we will attempt to discuss some of the key features of these approaches along with their shortcomings to the best of our understanding.

Homogenization is a well-established and mathematically consistent, theoretical framework for understanding multiscale problems. Earlier studies by [3, 34, 32, 17, 4] use homogenization theory for upscaling rapidly oscillating model parameters. For porous medium problems these parameters include rock properties such as permeability, porosity, dispersion as well as model parameters for relative permeability and heterogeneous chemical reactions. The two-scale homogenization theory relies upon the assumption of an identifiable period (or REV) in an otherwise heterogeneous medium with a characteristic length scale much smaller than the length scale of the medium under investigation. In other words, the ratio of the length of the period to the medium, denoted by ε, is sufficiently small. This assumption leads to a scale separation between fine and coarse scale problems thereby decoupling the computations associated with each of these two problems. The effective properties at the coarse scale can then be evaluated given fine scale parameters following the two-scale homogenization theory in the limit of $\varepsilon \to 0$. Please note that this passing to the limit is a theoretical construct, for determining convergence, and in practice a small value of ε suffices. However, the requirements of periodicity and scale separation are often too restrictive for direct application to realistic, heterogenous, porous medium problems. Nevertheless, homogenization is an indispensable mathematical tool in providing insight into the multiscale nature of the problem by describing coarse scale parameters as functions of fine scale variations. In fact, homogenization theory has been used successfully to derive [43, 33] the constitutive law, well known as Darcy's law, for porous medium continua starting from Stoke's (Navier-Stokes) equation at the pore scale. A derivation of the model problem at hand using two-scale homogenization is discussed in Section 3. As we will show later, numerical homogenization used appropriately allows us to recover fine scale features with minimal loss in accuracy.

A number of multiscale methods have been proposed, over the years, for a wide range of problems and include methods such as generalized finite elements [15], generalized multiscale finite element methods (GMsFEM) [29, 14, 22, 19], heterogeneous multiscale methods [2, 23], variational multiscale methods [31], mortar multiscale methods [11, 27, 16, 26]. A locally conservative mixed finite element, multiscale method was also presented in [7, 9]. Here, a subgrid problem is solved using a numerical approximation of Green's function which is later used as an operator for coupling coarse and fine scales.

In this work, we propose an adaptive homogenization approach using local numerical homogenization and adaptive mesh refinement to obtain computational efficiency and maintain solution accuracy. A fine scale problem is solved only in a subdomain of interest coupled to a coarse prob-

lem solve in the rest of the domain. This involves special treatment of sharp interfaces associated with phase (or component) transport equations. In this aspect, our method shares similarity with the adaptive [18] or hybrid [1] multiscale methods, discussed before, where a coarse problem is enriched locally to capture fine scale physical features. We define these sharp interfaces as transient regions or subdomains where spatial changes in concentration are significant. Away from the transient regions, upscaling is performed locally by using a numerical homogenization to obtain effective equations at the macroscopic scale. A fine spatial discretization is then used in the transient regions with a coarse discretization everywhere else resulting in a non-matching multiblock problem. An Enhanced Velocity Mixed Finite Element Method (EVMFEM) [42] is then used as a multiblock domain decomposition approach to solve this problem. EVMFEM has been shown to be both reliable and accurate [40], and is an order of magnitude faster than the Multiscale Mortar Mixed Finite Element Method (MM MFEM).

The remainder of this paper is organized as follows: Section 2 outlines flow and transport model formulation, Section 3 presents a derivation of effective equations at the coarse scale using two-scale homogenization followed by a brief outline of the EVMFEM for adaptive mesh refinement (AMR). The details of the proposed adaptive numerical homogenization approach are described in Section 4. This is followed by numerical results in Section 5 with verification numerical tests for numerical homogenization and AMR. Additional numerical tests, using realistic parameters from SPE 10 comparative project dataset, are also presented comparing fine scale, coarse scale using only numerical homogenization, and adaptive numerical homogenization solutions. Finally, Section 6 briefly presents conclusions based upon our study and an outlook towards future applications and extension.

2 Model formulation

We begin by describing the flow and transport model formulation along with initial and boundary conditions. We consider a single phase, slightly compressible fluid in porous medium with a non-reactive tracer transport for simplicity. The later transactions of this work will include more complex flow models such as non-linear, multiphase, multicomponent flow and detailed fluid compressibility models such as fully compressible and equation of state. The phase mass conservation equation on a domain Ω is given by,

$$\frac{\partial}{\partial t}(\phi\rho) + \nabla \cdot \rho \mathbf{u} = q \qquad \text{in} \quad \Omega \times J \tag{1}$$

Here, $\Omega \in \mathbb{R}^d (d = 1,2 \text{ or } 3)$, $J = (0,T]$, d is the number of spatial dimensions, q is the source/sink term, ϕ is the porosity, ρ is the phase density, and $\mathbf{u}$ is the phase velocity. The slightly compressible fluid density is defined as a function of pressure as follows,

$$\rho = \rho_{ref} e^{C_f (p - p_{ref})}, \tag{2}$$

where, C_f is the fluid compressibility, and ρ_0 is the reference density at reference pressure p_0. Then it follows that $\phi \frac{\partial \rho}{\partial t} = \phi \frac{\partial \rho}{\partial p} \frac{\partial p}{\partial t} = \phi \rho C_f \frac{\partial p}{\partial t}$ for constant ϕ. The phase velocity u is given by the Darcy's law as,

$$\mathbf{u} = -\frac{K}{\mu}(\nabla p - \rho \mathbf{g}), \tag{3}$$

where, μ is the viscosity, density, K is the permeability tensor, and $\mathbf{g}$ is the gravity vector. Further, the conservation equation of a component i in the flowing phase is given by,

$$\frac{\partial}{\partial t}(\phi c_i \rho) + \nabla \cdot (c_i \rho \mathbf{u} - \phi \rho D_i \nabla c_i) = q\hat{c}_i + \phi r_i, \tag{4}$$

where, c_i and D_i is the normalized concentration and diffusion/dispersion tensor, respectively of component i in the flowing phase and $\hat{c}_i$ is the injection/production concentration of the component i. We also define diffusive flux $\mathbf{d}_i$ for a component i as,

$$d_i = \phi D_i \nabla c_i, \tag{5}$$

for later use. The concentrations c_i are constrained by,

$$\sum_{i=1}^{N_c} c_i = 1. \tag{6}$$

For the sake of simplicity we assume Dirichlet and Neumann boundary conditions; for pressure and concentration, respectively, on the external boundary,

$$\begin{aligned} p &= g \quad \text{on} \quad \partial\Omega \times J \text{ ,} and \\ D_i \nabla c_i \cdot \nu &= 0 \quad \text{on} \quad \partial\Omega \times J, \end{aligned} \tag{7}$$

where *nu* is the unit outward normal;however, this is not restrictive and more general boundary conditions can be prescribed. Additionally, the initial condition is given by,

$$\begin{aligned} p(x,0) &= p^0(x) \\ c_i(x,0) &= c_i^0(x) \quad \text{at} \quad \Omega \times \{0\}. \end{aligned} \tag{8}$$

Eqns. (1) thru (8) describe a well posed problem for slightly compressible, single phase flow and transport in porous medium.

3 Methodology

In this work, we develop a local numerical homogenization scheme inspired by two-scale homogenization theory to obtain effective equations at the coarse scale starting from fine scale mass conservation equation and constitutive relationship (Darcy's law). Once the coefficients for the coarse scale equations are evaluated, we use a domain decomposition approach to couple coarse and fine subdomains. Further, details regarding the assumptions and validity of this approach to upscale flow and transport in heterogeneous porous medium is discussed in the next sections.

3.1 Two-Scale Homogenization

The two-scale homogenization theory relies upon two major assumptions to derive effective equations at the macroscopic scale:

1. An identifiable periodic REV at a mesoscopic scale of characteristic length l, with highly oscillatory (or heterogeneous) variations in parameters, in a macroscopic domain of another characteristic length scale L. These parameters include permeability, porosity as well as model parameters for heterogeneous chemical reactions.

2. A scale separation between the meso and macroscopic scales such that the ratio between the two characteristic length scales, discussed above, is small $\varepsilon = l/L \to 0$.

As stated before, $\varepsilon \to 0$ is a theoretical requirement for two-scale homogenization and in practice a small value of ε is sufficient for accurate numerical computations. The scale separation assumption here inherently implies that the pressure, velocity and concentration unknowns vary slowly (relatively non-oscillatory) at the macroscopic scale compared to faster variations (or highly oscillatory) at the mesoscopic scale.Under the aforementioned two-scale ansatz the unknowns in pressure, velocity and concentration are formally expanded as a power series in ε as,

$$a_\varepsilon(x) = a_0(x,y) + \varepsilon a_1(x,y) + \varepsilon^2 a_2(x,y) + ...$$

Here, a can be any one of the primary unknowns pressure (p) , velocity (u) or concentration (c). Further, x and y are the macro and mesoscopic scales such that $y = \frac{x}{\varepsilon}$ where $a(x,y)$ is used to denote the variations in an unknown at both the scales with periodic variations in $y \in Y$.

3.1.1 Flow

We begin by applying the two-scale homogenization theory to single phase slightly compressible flow problem in order to derive the effective flow equations at the macroscopic (or coarse) scale. The permeability and porosity are chosen as the highly oscillatory (or heterogeneous) parameters at the mesoscopic (or fine scale). In what follows, the terms mesoscopic and macroscopic can be used interchangeably with fine and coarse. The flow equations; for slightly compressible flow, at the fine scale have the following form,

$$\begin{aligned} \mathbf{u}_\varepsilon &= -\mathrm{K}\left(\frac{x}{\varepsilon}\right)\nabla p_\varepsilon \qquad \text{in } \Omega \\ \frac{\partial}{\partial t}(\phi\rho_\varepsilon) + \mathrm{div}\,(\rho_\varepsilon \mathbf{u}_\varepsilon) &= f \qquad \text{in } \Omega \\ p &= g \qquad \text{on } \partial\Omega \end{aligned} \tag{9}$$

where, ε denotes the two-scale variations in the unknowns $a_\varepsilon = a(x,y)$, $f \in L^2(\Omega)$ the source/sink term, and K and ϕ are the oscillatory (or heterogeneous) absolute permeability (symmetric, positive definite tensor) and porosity, respectively with period of oscillation $y = \frac{x}{\varepsilon}$. The two spatial scale x and y can be either in 2D or 3D. Additionally, the two-scale gradient and divergence operators are then defined as,

$$\nabla = \nabla_x + \frac{1}{\varepsilon}\nabla_y \qquad \mathrm{div} = \mathrm{div_x} + \frac{1}{\varepsilon}\mathrm{div_y}$$

Substituting, the formal expansion of the unknowns into the system of equations (9) we obtain,

$$\begin{aligned} &\mathbf{u}_0 + \varepsilon\mathbf{u}_1 + \varepsilon^2\mathbf{u}_2 + ... = -\mathrm{K}\left(\nabla_x + \frac{1}{\varepsilon}\nabla_y\right)\left(p_0 + \varepsilon p_1 + \varepsilon^2 p_2 + ...\right) \\ &\frac{\partial}{\partial t}\left(\phi\left(\rho_0 + \varepsilon\rho_1 + \varepsilon^2\rho_2 + ...\right)\right) + \left(\mathrm{div_x} + \frac{1}{\varepsilon}\mathrm{div_y}\right)\left(\rho_0 + \varepsilon\rho_1 + \varepsilon^2\rho_2 + ...\right)\left(\mathbf{u}_0 + \varepsilon\mathbf{u}_1 + \varepsilon^2\mathbf{u}_2 + ...\right) = f \end{aligned} \tag{10}$$

From the equations above, one can easily see that as $\varepsilon \to 0$, the unknowns $a_\varepsilon \to a_0$, or in other words the two scales are decoupled. Equating terms of like powers in ε in the above system provides us with effective equations at the coarse scale as follows,

1. For ε^{-1} terms:

$$-\mathrm{K}\nabla_y p_0 = 0$$
$$\mathrm{div_y}\left(\rho_0 \mathbf{u}_0\right) = 0$$

The solution to the above system results in $p_0(x,y) = p_0(x)$ which suggests that p_0 is only a function of coarse scale variations. In addition, we know that $\rho = \rho(p)$, or $\rho(p) = \rho_{ref} e^{C_f(p-p_{ref})} \approx p_{ref}\left(1 + C_f(p - p_{ref})\right)$.

$$\rho_0 + \varepsilon\rho_1 + \varepsilon^2\rho_2 + ... \approx p_{ref}\left(1 + C_f(p_0 + \varepsilon p_1 + \varepsilon^2 p_2 + ... - p_{ref})\right)$$

By equating terms in power of ε, we note $\rho_0 = p_{ref}\left(1 + C_f p_0(x,t) - p_{ref}\right)$. It implies $\rho_0 = \rho_0(x,t)$, and then $\mathrm{div_y}\left(\mathbf{u}_0\right) = 0$.

2. For ε^0 terms:

$$u_0 = -\mathrm{K}\left(\nabla_x p_0 + \nabla_y p_1\right)$$
$$\frac{\partial}{\partial t}\left(\phi\rho_0\right) + \mathrm{div_x}\left(\rho_0 \mathrm{u}_0\right) + \mathrm{div_y}\left(\rho_0 \mathrm{u}_1 + \rho_1 \mathrm{u}_0\right) = \mathrm{f}$$

Since u_0 is linear in p_0 and p_1, we can write $p_1(x,y,t)$ as,

$$p_1(x,y,t) = \sum_{i=1}^{3} \chi^i(y) \frac{\partial p_0}{\partial x_i}$$

In order to solve this system of equations we introduce an auxiliary problem, or a unit-cell problem for a dimensionless form of the above equations, on a periodic domain Y.

$$\begin{aligned} -\nabla \cdot \left(K(y)\left(\nabla\chi^i + e_i\right)\right) = 0 \quad \text{in } Y \\ \chi^i \text{ is perodic in } Y \end{aligned} \tag{11}$$

where $\{e_i\}_{1\le i\le d} \in \mathbb{R}^d$ is the canonical basis for a finite dimensional problem of dimension d. Note that the solution vector χ^i is unique up to a constant. We obtain uniqueness by normalizing the non-unique solution with the mean of the solution such that $\int_Y \chi^i(y)dy = 0$.

3. The effective or homogenized equations at the coarse scale are then obtained by averaging the above system of equations over periodic domain Y assuming $\varepsilon \to 0$.

$$\begin{aligned} \tilde{\mathbf{u}} &= -\mathrm{K}^{eff}\nabla p_0 && \text{in } \Omega \\ \frac{\partial}{\partial t}\left(\rho_0\langle\phi\rangle\right) + \mathrm{div_x}\left(\rho_0\tilde{\mathbf{u}}\right) &= f && \text{in } \Omega \\ p_0 &= g && \text{on } \partial\Omega \end{aligned} \tag{12}$$

Here, K^{eff} is a symmetric, positive definite tensor denoting the effective permeability at the coarse scale. Note that the effective permeability does not depend on the choice of domain Ω, source term f, and boundary conditions on $\partial\Omega$. Further, the eigenvalues of the effective permeability tensor are bounded below and above harmonic and arithmetic means of eigenvalues of the fine scale permeability tensors. [8] shows that the homogenized equations for the elliptic boundary value problem is well-posed which can be extended to the parabolic initial and boundary value problem

discussed above. The effective permeability tensor is constructed using the solution (χ^i) of the auxiliary problem Eqn. (11) as follows,

$$\vec{w}^i(y) = -K(y)\left(\nabla\chi^i + e_i\right) \text{ for } i = 1,..,d$$
$$Q(y) = [\vec{w}^1(y), \vec{w}^2(y), .., \vec{w}^d(y)]$$
$$K^{eff} = -\langle Q\rangle = -\frac{1}{|Y|}\int_Y Q(y)dy$$

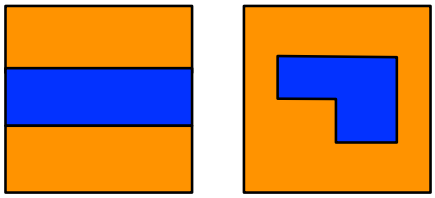

Figure 1: Schematic of REVs for layered (left) and general (right) permeability distribution.

An analytical derivation of effective permeability, using two-scale homogenization, for layered permeability distribution, with diagonal permeability tensor, is presented in [35]. This results in the well known arithmetic and harmonic averaging for flow along and across the layered medium, respectively. However, in order to use this result the REV must be chosen carefully so that the layered medium assumption and hence the aforementioned averaging applies. Figure 1 shows REV for layered and general distribution of permeability. One must note that it is not always possible to select an REV which satisfies the layered distribution wherein a more general approach such as numerical homogenization becomes indispensable. The numerical results section discusses the differences in results when the averaging approach for layered permeability REV is applied to a general heterogeneous case resulting in loss of connectivity of high perm channels.

3.1.2 Transport

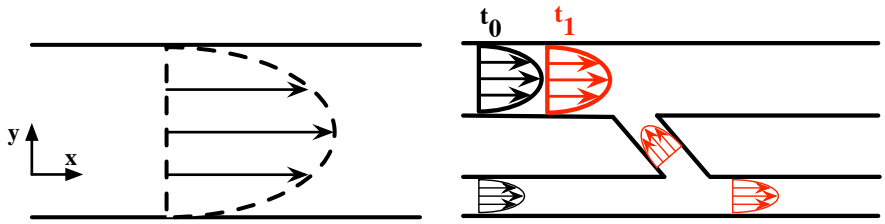

Figure 2: Example of Taylor (or hydrodynamic) dispersion (left) and mechanical mixing (right).

In this section we begin by discussing three important aspects of component transport namely: diffusion, mechanical dispersion, and mechanical mixing. The physical process of molecular diffusion (or simply diffusion), due to spatial differences in concentration, is well accepted to follow Fick's law,

$$J_i = -D_i \nabla c_i. \tag{13}$$

Here, J_i is the diffusive flux of component i, and D_i the diffusivity constant D_i defined with respect to a reference component, water component (or phase) in our case. The dispersion phenomenon was first described mathematically by Taylor [39] for laminar, miscible flow of a component in a cylindrical tube. The additional diffusion (or mechanical dispersion) in the longitudinal direction, after model reduction to a one-dimensional flow and transport, was attributed to the Fickian diffusion in the transverse direction. For further details regarding the derivation the reader is referred to the original text [39]. There are two interesting features necessary for mechanical dispersion to be non-zero: (1) a velocity profile, parabolic in the case of fully developed laminar flow in a tube, and (2) a non-zero molecular diffusion. Absence of either one of the above two features results in a zero dispersion. Figure 2 (left) shows a schematic of the fully developed parabolic velocity profile in a cylindrical tube. The x-direction velocity is maximum at the centre of the tube and zero at the solid boundary consistent with the no-slip assumption at the solid fluid boundary. Taylor described the diffusion in the y-direction, due to difference in concentration at the fluid front, to be responsible for the additional diffusion in the x-direction after a model reduction was performed in the y-direction. In fact, the sum of molecular diffusion and mechanical dispersion is well known as hydrodynamic dispersion in several scientific communities. Similar arguments have been used for dispersion in porous medium where differences in velocity, due to heterogeneity, at the concentration front leads to additional diffusion. Therefore, a negligible diffusion coefficient will consequently lead to a small mechanical dispersion for flow and transport in porous medium as well.

On the contrary, the same cannot be said about mechanical mixing that also results from heterogeneities in porous medium. Figure 2 (right) shows a schematic of mechanical mixing for a simple case of miscible laminar flow in two cylindrical tubes connected in the middle. We assume that the velocity in the larger diameter tube is smaller, compared to the smaller diameter tube, and therefore the concentration front moves slower in the former. Let the black and red colors represent the concentration fronts at times t_0 and t_1. It is clear that the two concentration fronts would merge into one another due to this interconnectivity. Similar arguments can be extended for heterogeneous porous medium where differences in permeability and connectivity can result in mechanical mixing to different degrees. This connectivity is usually characterized by a scalar quantity, called tortuosity, for a porous continuum. Please note that mechanical mixing and spreading can exist even in the absence of molecular diffusion and are usually an order of magnitude larger than molecular diffusion. In this work, we can account for all three phenomena using an AMR approach to accurately capture the concentration front. This is necessary since homogenization approaches for advection/diffusion problem; although accurate, are computationally as expensive as solving the a local fine scale problem.

A similar discourse as in the case of homogenizing flow equations above is applied to the advection/diffusion problem Eqn. (4) to obtain the effective equations at the macroscopic scale described below. Here we briefly discuss the derivation of these equations; following the original work in [4], for the sake of completeness. Since $\rho_0 = \rho_0(x)$ or the ε^0 order density varies only at the coarse scale, the derivation of effective transport equations for slightly compressible flow remains unchanged from the original derivation for incompressible flow. The dimensionless form of the

transport equation is given by,

$$\begin{aligned} \phi\left(\frac{x}{\varepsilon}\right)\frac{\partial c_\varepsilon}{\partial t}+\mathbf{u}^\varepsilon\cdot\nabla c_\varepsilon=\frac{\varepsilon}{Pe}\nabla\cdot\left(D\left(\frac{x}{\varepsilon}\right)\nabla c^\varepsilon\right) \qquad & \text{on} \quad \Omega\times J, \\ c_\varepsilon(x,0)=c^0(x) \qquad & \text{on} \quad \Omega\times\{0\}. \end{aligned} \tag{14}$$

Using the two-scale ansatz,

$$\begin{aligned} c_\varepsilon(x)&=c_0(x,y)+\varepsilon c_1(x,y)+\varepsilon^2 c_2(x,y)+..., \\ \mathbf{u}_\varepsilon(x)&=\mathbf{u}_0(x,y)+\varepsilon\mathbf{u}_1(x,y)+\varepsilon^2\mathbf{u}_2(x,y)+.... \end{aligned}$$

Substituting these expansions we obtain,

$$\begin{aligned} \phi\frac{\partial}{\partial t}(c_0+\varepsilon c_1+...)+(\mathbf{u}_0+\varepsilon\mathbf{u}_1+...)(\nabla_x+\frac{1}{\varepsilon}\nabla_y)(c_0+\varepsilon c_1+...) \\ =\frac{\varepsilon}{Pe}(\mathrm{div}_x+\frac{1}{\varepsilon}\mathrm{div}_y)D(\nabla_x+\frac{1}{\varepsilon}\nabla_y)(c_0+\varepsilon c_1+...) \end{aligned}$$

Collecting terms of the same ε-order gives

1. For ε^{-1} terms:

   $$\mathrm{div}_y(D\nabla_y c_0)-\mathbf{u}_0\cdot\nabla_y c_0=0$$

   As before, this implies $c_0=c_0(x,t)$.

2. For ε^0 terms we take into account that $c_0=c_0(x,t)$:

   $$\phi\frac{\partial c_0}{\partial t}+\mathbf{u}_0\cdot\nabla_x c_0+\mathbf{u}_0\cdot\nabla_y c_1=\frac{\varepsilon}{Pe}\mathrm{div}_y\left(D\nabla_y c_1\right) \tag{15}$$

   The homogenized equation; for ε^0 order accuracy in concentration, is obtained by integrating over the fine scale (Y),

   $$\langle\phi\rangle\frac{\partial c_0}{\partial t}+\langle\mathbf{u}_0\rangle\cdot\nabla_x c_0=0, \tag{16}$$

   where, $\langle w\rangle=\int\limits_Y w dy$

3. For ε^1 terms:

   $$\phi\frac{\partial c_1}{\partial t}+\mathbf{u}_0\cdot\nabla_y c_2+\mathbf{u}_1\cdot\nabla_x c_0+\mathbf{u}_1\cdot\nabla_y c_1=\frac{1}{Pe}\left(\mathrm{div}_x\left(D\nabla_x c_0+D\nabla_y c_1\right)+\mathrm{div}_y\left(D\nabla_x c_1+D\nabla_y c_2\right)\right) \tag{17}$$

   Similarly the homogenized equation; for ε^1 order accuracy in concentration, is given by,

   $$\langle\phi\rangle\frac{\partial c_\varepsilon^1}{\partial t}+\langle\mathbf{u}_0\rangle\cdot\nabla_x c_\varepsilon^1=\frac{\varepsilon}{Pe}\mathrm{div}_x\left(D^{eff}\nabla_x c_\varepsilon^1\right). \tag{18}$$

   Here, c_ε^1 is the macroscale concentration defined as $c_\varepsilon^1(x,t)=c_0+\varepsilon c_1$, D^{eff} the effective diffusivity tensor, $\langle\phi\rangle$ the volume averaged porosity, $\langle u_0\rangle$ the effective Darcy velocity, and Pe the Peclet number.

3.2 Enhanced Velocity Mixed FEM

Mixed Finite Element Method (MFEM) was initially introduced as a spatial discretization scheme by the engineering commy [20, 28] in the late 70s for solving problems in solid continua. For flow in porous medium, the cell-centered finite difference scheme goes back to 50s and was later shown to be a mixed method in the early 80s by [37, 41]. Later works have applied this scheme for a wide range of applications in multicomponent, multiphase fluid flow [40, 13, 38] and transport, as well as coupled flow and geomechanics [5, 6] in porous medium. The mixed scheme uses a high-order approximation for both pressure and velocity variables resulting in accurate fluxes and local mass conservation properties. Enhanced Velocity MFEM [42] and Multiscale Mortar Mixed Finite Element Method (MM MFEM) [11, 36, 12] are spatial domain decomposition approaches to handle non-matching, multi-block grids. MM MFEM has been used to accurately couples different flow physics in different subdomains through interface conditions; however, this results in an additional nested iteration loop for interface problems. The EV MFEM approach, on the other hand, is shown to have an order of magnitude faster performance, with similar accuracy, when compared to the mortar approach. Recently, a global Jacobian method for mortar discretization [25] of two-phase flow was developed that obtains similar computational efficiency compared to the original MM MFEM solution algorithm. Additionally, this approach is strongly mass conservative at the interfaces; strong continuity of fluxes, between the subdomains.

EV MFEM has been applied successfully to a wide variety of complex multicomponent, multiphase flow and transport processes in porous medium including equation of state (EOS), compositional flow [40]. Earlier implementations [42, 40] employed a solution approach where only the coarse and fine domain contributions to the stiffness-matrix (or Jacobian matrix) were taken, neglecting interface contributions. The load vector (or residuals); however, contains contributions from both the coarse and fine subdomains as well as the interface. This resulted in an increase in the number of non-linear iterations to achieve convergence, for a given tolerance, even for a linear flow and transport problem. In this work, we use a fully coupled variant of the original EV MFEM approach wherein the interface terms are properly accounted for in the stiffness-matrix construction resulting in reduced non-linear iterations (one for a linear system).

3.2.1 Enhanced Velocity Mixed FEM Scheme

In this subsection, we briefly reiterate some parts of the derivation, presented in [40], for the multi-block, domain decomposition approach EV MFEM. This derivation is an extension of the original work by [42] for an incompressible, elliptic flow equation to a slightly compressible, parabolic flow system. The partial differential equations associated with a slightly compressible flow system, along with initial and boundary conditions, is described before in Section 2. We begin by describing the spaces for the velocity and pressure unknowns as,

$$\begin{aligned}
&\mathbf{V} = H(\mathrm{div};\Omega) = \{\mathbf{v} \in \left(L^2(\Omega)\right)^d : \nabla\cdot\mathbf{v} \in L^2(\Omega)\},\\
&W = L^2(\Omega),
\end{aligned}$$

equipped with the following norms,

$$\begin{aligned}
&\|\mathbf{v}\|_V = \left(\|\mathbf{v}\|^2 + \|\nabla\cdot\mathbf{v}\|^2\right)^{\frac{1}{2}},\\
&\|w\|_W = \|w\|.
\end{aligned}$$

A weak solution of Eqns. (1)-(8), excluding the advection diffusion and concentration constraint, is the pair $\mathbf{u} \in L^2(J,V)$ and $p \in H^1(J,W)$ obtained by solving,

$$\left(K^{-1}\mathbf{u},\mathbf{v}\right) = (p,\nabla\cdot\mathbf{v}) - <g,\mathbf{v}\cdot\nu>_{\partial\Omega} \qquad \forall \mathbf{v}\in\mathbf{V}, \tag{19}$$

$$\left(\phi C_f \frac{\partial p}{\partial t}, w\right) + (\nabla\cdot\rho\mathbf{u}, w) = (f,w) \qquad \forall w \in W. \tag{20}$$

Also, the initial condition

$$(p,w)\Big|_{t=0} = (p_0,w) \qquad \forall w \in W \tag{21}$$

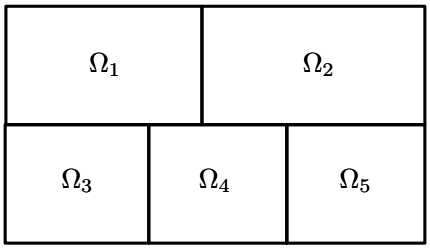

Figure 3: Spatial domain decomposition into multi-block problem.

Let denote $\Gamma_{i,j} = \partial\Omega_i \cap \partial\Omega_j$ denote the interface between subdomains Ω_i and Ω_j then $\Gamma = \cup_{i,j=1}^{n}\Gamma_{i,j}$ and $\Gamma_i = \Omega_i \cap \Gamma = \partial\Omega_j \setminus \partial\Omega$. The subdomain partitions, or the grid elements in each subdomain, $\mathscr{T}_{h,i}$ and $\mathscr{T}_{h,j}$ need not match on $\Gamma_{i,j}$ then, $\mathscr{T}_h = \cup_{i=1}^{n}\mathscr{T}_{h,i}$. We use the RT_0 and piecewise constant finite-element space for the velocity and pressure unknowns defined on an element $E \in \mathscr{T}_h$ as,

$$V_h(E) = \{\mathbf{v} = (v_1,v_2)\ or\ \mathbf{v} = (v_1,v_2,v_3) : v_l = \alpha_l + \beta_l x_l : \alpha_l,\beta_l \in \mathbb{R}; l = 1,..d\},$$

and

$$W_h(\Omega) = \{w \in L^2(\Omega) : w\Big|_E \in W_h(E), \forall E \in \mathscr{T}_h\}$$

, respectively. The EV MFEM scheme modifying the degrees of freedom on the interface Γ to accommodate the non-matching flux degrees of freedom from the adjacent blocks, as shown in Figure 4. Let $\tau_{h,i,j}$ be a rectangle partition of $\Gamma_{i,j}$ obtained from intersection of the traces of $\mathscr{T}_{h,i}$ and $\mathscr{T}_{h,j}$. The enhanced velocity scheme forces the fluxes to match on each element edge $e \in \tau_{h,i,j}$.

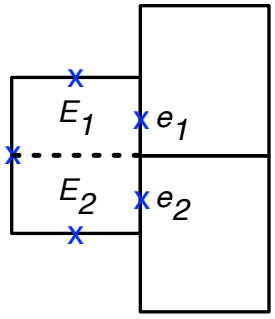

Figure 4: Degrees of freedom for the Enhanced Velocity Space.

On each sub-element E_k a basis function $\mathbf{v}_{E_k}$ is defined belonging to the RT_0 space $\mathbf{V}_h(E_k)$ as follows,

$$\mathbf{v}_{E_k} \cdot \nu = \begin{cases} 1 & \text{on } e_k, \\ 0 & \neq e_k. \end{cases}$$

Let $\mathbf{V}_h^\Gamma$ be span of all such basis functions. Then the multiblock mixed finite element velocity space is given by,

$$\mathbf{V}_h^* = \left(\mathbf{V}_{h,1}^0 \oplus \mathbf{V}_{h,2}^0 \oplus \cdots \oplus \mathbf{V}_{h,n}^0 \oplus \mathbf{V}_h^\Gamma\right) \cap H(\text{div};\Omega).$$

Here, $\mathbf{V}_{h,i}^0$ is the subspace of $\mathbf{V}_{h,i}$ with zero normal trace on Γ_i. Also note that $\mathbf{V}_h^* \subset H(\text{div};\Omega)$. The variational problem in discrete space can then be written as: Find $u_h \in L^2\left(J, \mathbf{V}_h^*\right)$ and $p_h \in H^1\left(J, W_h\right)$ such that,

$$\left(K^{-1}\mathbf{u}_h, \mathbf{v}\right) = \left(p_h, \nabla \cdot \mathbf{v}_h\right) - < g, \mathbf{v}_h \cdot \nu >_{\partial\Omega} \qquad \forall \mathbf{v}_h \in \mathbf{V}_h^*, \quad (22)$$

$$\left(\phi \rho_0 C_f \frac{\partial p_h}{\partial t}, w_h\right) + \left(\nabla \cdot \rho(p_h)\mathbf{u}_h, w_h\right) = \left(f, w_h\right) \qquad \forall w_h \in W_h. \quad (23)$$

The existence and uniqueness of this problem is shown in [42] for the elliptic case without applying the inf-sup condition directly. Here, error estimates were also derived for the problem at hand and a first order convergence was shown. We reiterated some of the earlier developments of EV MFEM for single phase flow, next we extend this scheme for the transport or the advection/diffusion problem Eqn. (4), similar to [40]. Let us define, $\mathbf{V}_h^{*,0} \equiv \mathbf{V}_h^* \cap \{\mathbf{v} : \mathbf{v} \cdot \nu = 0 \text{ on } \partial\Omega\}$. The discrete variational problem; using the enhanced velocity space $\mathbf{V}_h^{*,0}$ for the diffusive/dispersive flux, is: Given $u_h \in L^2\left(J, \mathbf{V}_h^*\right)$ and $p_h \in H^1\left(J, W_h\right)$, find $\mathbf{d}_{i,h} \in L^2\left(J, \mathbf{V}_h^{*,0}\right)$ and $c_{i,h} \in H^1\left(J, W_h\right)$ such that,

$$\left(\frac{1}{\phi} D_i^{-1} \mathbf{d}_{i,h}, \mathbf{v}_h\right) = \left(c_{i,h}, \nabla \cdot \mathbf{v}_h\right) \qquad \forall \mathbf{v}_h \in \mathbf{V}_h^{*,0}, \quad (24)$$

$$\left(\phi \rho_0 C_f \frac{\partial p_h}{\partial t} c_{i,h}, w_h\right) + \left(\phi \rho(p_h) \frac{\partial c_{i,h}}{\partial t}, w_h\right) + \left(\nabla \cdot \rho(p_h)\mathbf{u}_h c_{i,h}, w_h\right) - \left(\nabla \cdot \rho(p_h)\mathbf{d}_{i,h} c_{i,h}, w_h\right) = \left(f, w_h\right) \qquad \forall w_h \in W_h. \quad (25)$$

In the above, we assume $D_i > 0$. The EV MFE method ensures that both advective and diffusive fluxes are strongly continuous at the subdomain interfaces for this domain decomposition approach

to be locally mass conservative. For single phase flow and tracer transport, the flow problem is inherently decoupled from the transport problem and therefore these two problems can be solved consecutively, as shown above. However, a fully coupled form can also be described as: Find $u_h \in L^2\left(J, \mathbf{V}_h^*\right)$, $p_h \in H^1\left(J, W_h\right)$, $\mathbf{d}_{i,h} \in L^2\left(J, \mathbf{V}_h^{*,0}\right)$, and $c_{i,h} \in H^1\left(J, W_h\right)$ such that, Eqns. (22) thru (25) are satisfied.

4 Adaptive Homogenization

The adaptive homogenization approach presented here has two key steps: (1) numerical homogenization to obtain parameters (permeability, porosity etc.) at the coarse scale by solving local auxiliary problems, (2) use enhanced velocity for AMR, with coarse and fine mesh regions identified using an adaptivity criteria, to solve coupled flow and transport problems. The subsections below describe the numerical homogenization and transient region identification using an indicator function. Here, a backward Euler scheme is used for temporal discretization resulting in a fully implicit system with spatial discretization using the fully-coupled, enhanced velocity mixed finite element method described in subsection 3.2. Since the solution scheme is fully implicit in pressure and concentration there is no time-step size restriction, as in the case of an explicit scheme where a CFL criteria is used. Further, an upwinding scheme is used for the advective flux term (uc_i); to add sufficient diffusion, for the stability of the concentration solution.

4.1 Numerical Homogenization

We first perform numerical homogenization to obtain coarse scale parameters for a given set of fine scale properties. Here, we solve local auxiliary problem, Eqn. (11), using fine scale parameters on a set of subdomains with periodic boundary conditions to evaluate coarse scale parameters. The term local here is used to differentiate between numerical homogenization, for a globally periodic medium with a characteristic length scale, as opposed to a locally periodic or non-periodic medium. Figure 5 depicts global and local periodicities in porous medium. Please note that this figure is only for the purpose of illustration and the shapes of the microstructures chosen are of no consequence. These local periodicities are often observed in well log data where each layer represents a sedimentation and consolidation cycle.

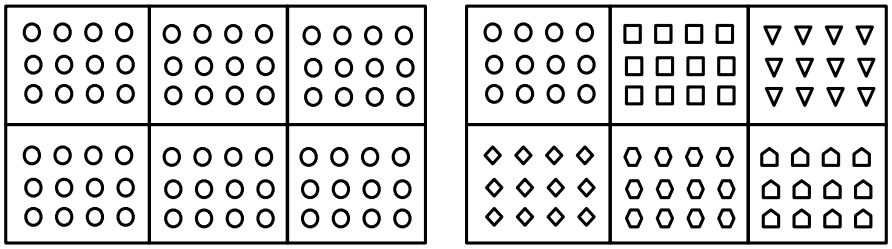

Figure 5: Globally (left) and locally (right) periodic medium.

Figure 6 shows the horizontal permeability distribution for the Frio field pilot injection well

obtained from well-logging [30] . The orange and blue zones identify the high and low permeability regions in the well log which allude to periodicity. Although, such an assumption is only valid for near well-bore parameters (permeability, porosity etc.) characterized by a specific length scale. The periodic porous medium is a convenient construct for mathematical analysis; however, such an assumption is not always valid for realistic subsurface porous media problems. The reader is referred to [4] for further details regarding where a scale separation and periodicity is necessary for the theoretical framework or two-scale homogenization. In our work, we consider highly heterogeneous flow parameters where these assumptions do not apply.

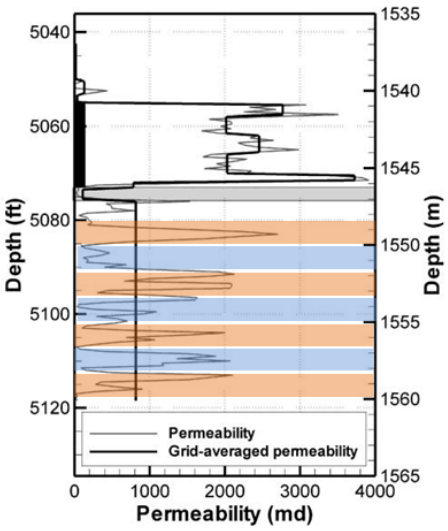

Figure 6: Horizontal permeability distribution with depth for Frio field injection well.

Figure 7 shows a schematic of this local numerical homogenization where auxiliary problems are solved on a subdomain (Figure 7, Ω_i, dotted red, left) at the fine scale. Each of these cell problems provides a coarse scale parameter on the coarse grid (Figure 7, dotted red, right). These calculations are called offline since they are performed as a pre-processing step once prior to the actual numerical simulations.This approach works well since the non-linearity introduced due to slightly compressible flow model is quite small. Since we consider single phase slightly compressible flow with transport this approach works well since the non-linearity introduced by considering a slightly compressible flow model is quite small. For non-linear problems, these calculations must either be performed online, or in other words during numerical simulation run. However, there are other alternatives in the case of multiphase flow which allow us to store these parameters in a functional form evaluated again as a pre-processing or offline step. This latter methodology will be present in our future works for two-phase oil-water or air-water systems. Subsection 5.1 in the numerical results section presents two examples where only numerical homogenization is used, without adaptivity, for both periodic and non-periodic media.

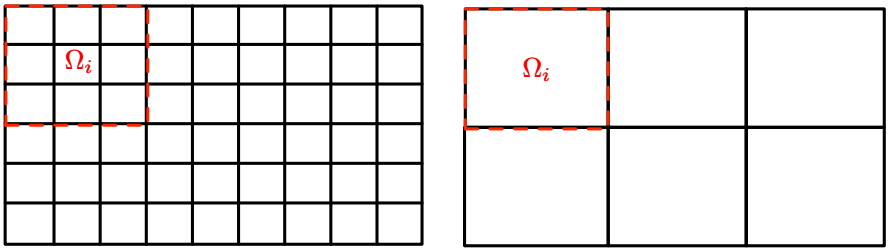

Figure 7: Schematic of numerical homogenization to obtain coarse scale (right) parameters from fine scale (left).

In the adaptive homogenization approach presented here, we use these coarse scale properties only in the non-transient region, identified by an indicator function. This indicator function (or adaptivity criteria) and further details regarding transient/non-transient demarcation are presented in the next subsection.

4.2 Transient Region Identification/Adaptivity Criteria

For multicomponent, multiphase, flow and transport in porous medium the accuracy of the numerical solution depends upon how accurately the concentration front is captured. In order to capture the front accurately, the fluid velocities must be resolved accurately along this concentration front since the component is transported by the fluid velocity. This necessitates that a fine scale problem be solved, with fine scale properties for flow and transport, in the vicinity of the front for accuracy. The computational overheads are reduced by solving a coarse scale problem away from the transient region using coarse scale properties obtained from numerical homogenization. We therefore define a transient region in space where the changes in concentration are larger than a given threshold. This notion has also been used earlier by several others [1] to reduce computational costs associated with different problems. For example, in compositional flow modeling, the local equilibrium computations (flash calculations) are performed based upon the identification of a spatial transient region where a given fluid composition splits into multiple phases. In this work, we use the following adaptivity criteria to identify the transient region for spatial domain decomposition,

- Criteria 1 (gradient in time): For a block i we know c at previous timesteps n and $n-1$. An adaptivity criteria can be defined based upon an absolute of the difference between the previous time steps as,

$$\Omega_f = \left\{ \mathbf{x} : |c^n(x) - c^{n-1}(x)| > \varepsilon_{tadap} \right\} \tag{26}$$

- Criteria 2 (gradient in space): A similar criteria can be defined in space using a maximum of absolute of difference between a concentration c and its adjacent neighbors at the previous time step n. We define $\Omega_{neighbor}(x) = \{y : y \in E_j, |\partial E_i \cap \partial E_j| \neq \emptyset, \text{if } x \in E_i\}$. The criteria can then be defined as,

$$\Omega_f = \left\{ \mathbf{x} : \max|c^n(x) - c^n(y)| > \varepsilon_{sadap} \quad \forall y \in \Omega_{neighbor}(x) \right\} \tag{27}$$

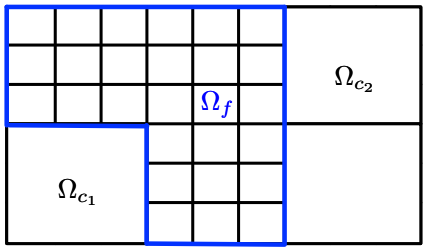

Figure 8: Schematic of adaptive mesh refinement with coarse (Ω_c) and fine (Ω_f) domains.

Based upon this criteria we divide the domain (Ω) into non-overlapping, transient (Ω_f) and non-transient (Ω_c) subdomains where flow and transport problems are solved at the fine and coarse scales, respectively. Figure 10 shows a schematic of the domain decomposition approach used here. In what follows, coarse and non-transient, and fine and transient can be used interchangeably to refer to a subdomain. Further, the coarse and fine subdomain problems are coupled at the interface using the EVMFEM spatial discretization described earlier in section 3.2. The EV MFEM method is strongly mass conservative at the interface between fine and coarse domains.

4.3 Solution Algorithm

This subsection describes the solution algorithm for the adaptive homogenization approach discussed above. The local unit-cell (auxiliary) problems are solved as a pre-processing step to evaluate coarse scale coefficients using numerical homogenization. This step can be carried out in parallel to further improve computational efficiency since the unit-cell problems are mutually independent. We refer to this calculation as the offline stage since the parameters (permeability, porosity, etc.) remain temporally invariant. Please note that such an assumption is true only for incompressible and slightly compressible single phase flow and transport models and further considerations are needed for highly non-linear multiphase, multicomponent flow and reactive transport problems. In such cases, the local unit-cell problem will be solved as time evolves to re-evaluate (online stage) coarse scale coefficients in a subdomain identified by a different indicator function. We reserve further details regarding this approach to our future extension to multiphase systems.

Algorithm 1 Adaptive multi-scale solution algorithm for the coupled flow and transport problem

Solve unit-cell problems, Eqns. (11), on subdomains (Ω_i) using fine scale parameters to obtain coarse scale parameters for the entire domain ($\Omega = \cup\Omega_i$, see Figure 5).

while $t_n \leq T$ **do**

Identify transient (Ω_f) region using adaptivity criteria (Eqn. (26) or (27)) and p, c at t_n ($\Omega_f \cup \Omega_c = \Omega$).

Mass conservative initialization of primary unknowns:

1. Reconstruct primary unknowns $p^{n+1,0}, c^{n+1,0}$ for the fine scale transient region (Ω_f).
2. Project primary unknowns $p^{n+1,0}, c^{n+1,0}$ for the coarse scale non-transient region (Ω_c).

while $max(\vec{R}_{nl}) > \varepsilon_{nl}$ **do**

1. Use fine and coarse scale parameters in the transient (Ω_f) and non-transient (Ω_c) regions, respectively.
2. Use enhanced velocity (EV) scheme to couple coarse and fine subdomains.
3. Solve linearized, algebraic system for the coupled flow and transport problem to obtain a Newton update $p^{n+1,k+1}, c^{n+1,k+1}$.

end

$t_{n+1} = t_n + \Delta t$, $n := n + 1$

end

Flowchart 1 shows a brief outline of the solution algorithm. Here, n and k are the time and non-linear iteration counter, t_n and t_{n+1} are the current and next time, Δt current time-step size, T the final time, $max(\vec{R}_{nl})$ the max norm of the non-linear residual vector, and ε_{nl} the non-linear tolerance. At each time iterate, we evaluate the adaptivity criteria (Eqn. (26) or (27)); at the coarse scale, to identify the transient region and perform a domain decomposition into fine (Ω_f) and coarse Ω_c subdomains. A projection/reconstruction operation is performed if the identifier changes from coarse to fine or vice versa, respectively. The reconstruction is performed by simply using previous time step unknowns and since these are intensive properties the operation remains mass conservative. On the other hand a mass conservative projection (L^2 projection) is used for coarsening which is equivalent to arithmetic average of fine scale unknown (p, c) for incompressible flow. This is followed by a non-linear solve of the system of algebraic equations resulting from spatial and temporal discretization after domain decomposition. The non-linear iterations are performed until the max norm satisfies a desired tolerance corresponding to the error in phase and component mass conservation equations.

5 Numerical Results

As mentioned in earlier, we avoid additional calculations due to changes in process parameters using a mass conservative, AMR based upon the fully coupled enhanced velocity approach. This also

helps us to generalize the adaptive homogenization approach towards making it process independent. In this section, we present two sets of numerical results for (1) numerical homogenization, and (2) adaptive homogenization with one verification case for each set. The tracer production curves are reported for each of the cases to demonstrate the effectiveness of the two approaches in capturing the fine scale flow and transport physics. The heterogenous porous medium is extracted from the SPE 10 comparative project for benchmarking different upscaling approaches. We report speedups by comparing coarse and fine scale simulation runtimes. One important point to note here is that the speedup factors reported here takes into account the computational overheads due to the pre-processing step.

5.1 Numerical Homogenization

We first verify the numerical homogenization approach using a periodic medium followed by a local numerical homogenization on a highly heterogeneous (non-periodic) medium. The results are compared against fine scale simulations as the benchmark. The reservoir domain is 110ft $\times$ 30ft with fine scale permeability distribution available for a 220×60 grid with grid block size $0.5\text{ft}\times0.5\text{ft}$. A coarse scale permeability distribution for a 22×6 grid is obtained by two-scale homogenization, as a preprocessing step at the beginning of the simulation, with grid block size of $5\text{ft}\times5\text{ft}$. Here a local cell problem, for a 10×10 grid, with periodic boundary conditions is solved at the fine scale. A rate specified injection well and pressure specified production well are located at the bottom left and top right corner, respectively. The production pressure is specified at 1000 psi with a continuous tracer injection at concentration 1. The initial reservoir pressure and concentrations are taken to be 1000 psi and zero (mass fraction), respectively with a fluid compressibility of 1×10^{-6} psi $^{-1}$. All simulations were performed for a total duration of 200 days with a no-flow external boundary condition.

Verification: Periodic Medium

We define a periodic medium where each period is characterized by a high permeability lens K_{xx} = 50 mD, K_{yy} = 100 mD in a low permeability porous matrix $K_{xx} = 5mD, K_{yy} = 10mD$. Figure 9 shows the global and local permeability distributions for the periodic medium and the unit cell, respectively. We assume diffusion to be zero in this case for simplicity; however, a separate case considering non-zero diffusion is also presented. Further, a homogeneous reservoir porosity of 0.1 is considered with incompressible fluid description and an injection rate specification at 2 STB/day.

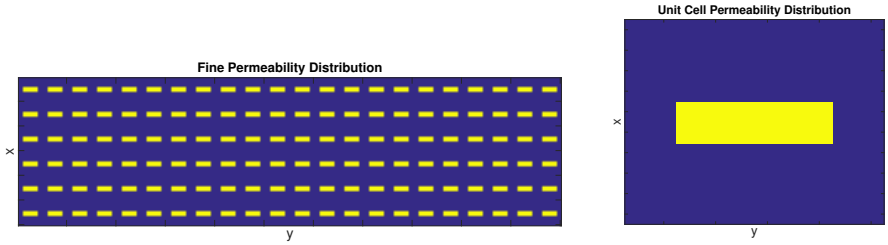

Figure 9: Global (left) and unit cell (right) permeability distributions.

Figure 10 shows the fine and coarse scale concentration profiles after 100 days of simulation run.

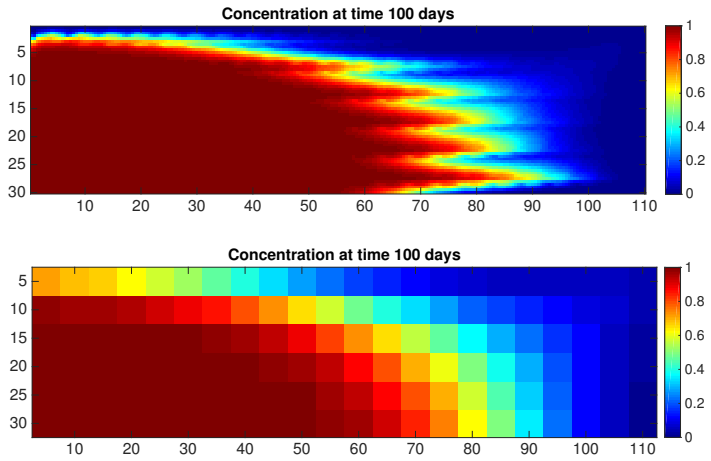

Figure 10: Concentration distributions for fine (top) and coarse (bottom) scale problems after 100 days.

Further, Figure 11 shows the tracer concentration history at the production well for the fine and coarse (or homogenized) cases. The fine and coarse scale results are in good agreement for this benchmark verification case. The coarse scale simulation run is approximately 40 times faster than the fine scale run which is attributed to the reduction in degrees of freedom (factor of 100) for the coarse scale simulation.

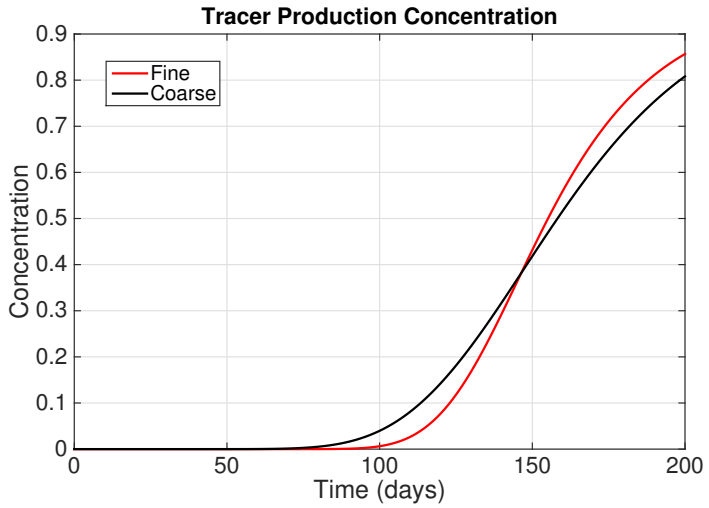

Figure 11: Tracer production history for Fine and coarse (homogenized) scale problems.

Non-Periodic Medium

Here, we consider a highly heterogeneous, non-periodic medium with respect to permeability and porosity distribution. We utilize the SPE10 comparative project for benchmarking upscaling approaches to obtain this distribution from layer 81 of the available dataset. Figure 12 shows one fine scale , from SPE10 layer 81, and two coarse scale permeability distributions obtained using local numerical homogenization and local harmonic averaging, respectively. A channelized permeability distribution can be seen with high contrast in permeability values varying over 6 orders in magnitude. Please note that the coarse scale permeabilities obtained using numerical homogenization preserve the channels, observed at the fine scale, as opposed to the harmonic averaging. Injection rate is 1 STB/day.

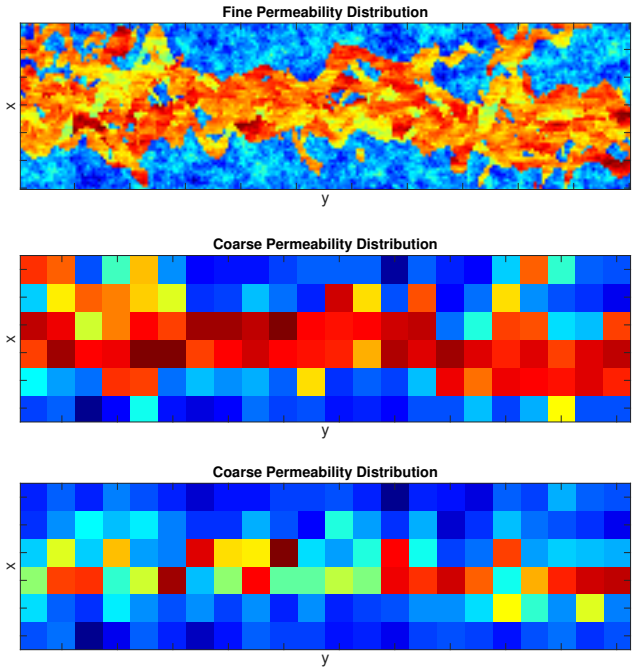

Figure 12: Permeability distributions for fine (top) and coarse homogenized (middle) and coarse harmonic (bottom) cases of SPE layer 81.

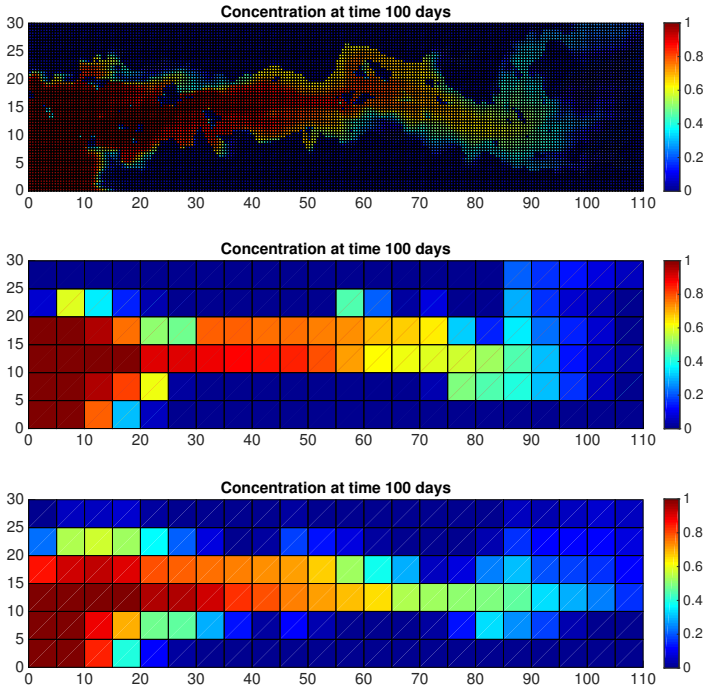

Figure 13: Concentration distributions for fine (top) and coarse homogenized (middle) and coarse harmonic (bottom) scales of SPE layer 81.

Figure 13 shows the concentration profiles for the three cases after 100 days of continuous tracer injection. As can be seen, the concentration profile for the harmonic average differs from the fine scale solution. This is clearly evident in the tracer concentration history, in Figure 14, where the harmonic average result deviates from the fine scale solution. Although, not a perfect match the numerical homogenization solution is closer to the fine scale solution even after a reduction in degrees of freedom from 26400 to 264 (factor of 100). The speedup is approximately 40 times, which is roughly the same as in the previous case.

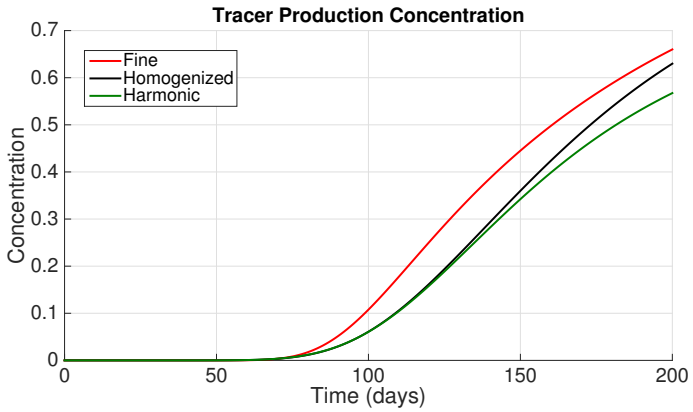

Figure 14: Tracer production history for fine and coarse (homogenized and harmonic average) scale problems.

5.2 Adaptive Numerical Homogenization

In this section, we compare numerical results for the fine scale and coarse scale using the adaptive homogenization and numerical homogenization approaches, respectively. We begin with by numerically verifying the AMR using a benchmark homogeneous case. We observed a speedup of at least 4 times for all the adaptive homogenization cases below when compared to fine scale case. Certainly, the speedup can be increased further by lowering the tolerance of the adaptivity criteria however, this also results in reduced solution accuracy. Thus an optimal tolerance exists which provides a breakeven between solution accuracy and computational speedup. We also outline a procedure for identifying this optimal tolerance for which calculations can be performed as a pre-processing step.

The reservoir domain, initial and boundary conditions, well placement and specifications are kept the same as in the previous subsection. However, instead of a continuous tracer injection a tracer slug is injected for a period of 50 days at concentration 1. Further, the injection rate is chosen to be 1 STB/day for a total simulation time of 200 days. The heterogeneous permeability distributions are obtained from different layers of the SPE10 comparative project dataset. Although, porosity distributions are not shown here the coarse scale porosities were obtained from fine scale distributions by applying a simple volume averaging, Eqn. (16). In what follows we choose two permeability distributions from SPE10 dataset: (1) layer 20 and (2) layer 37 with injection and production specified at the bottom left and upper right corners. It is important to note here that the accuracy of the solution, compared to the benchmark fine scale solution, can be increased further by using a stricter criteria for adaptivity in all of the following results.

Verification: Homogeneous Case

A homogeneous, isotropic permeability distribution is assumed using a diagonal permeability tensor of 50 mD to verify the adaptive solution against fine scale solution. This numerical test differs only in the injection rate, taken to be 2 STB/day instead of the 1 STB/day, from all the other cases in what follows.

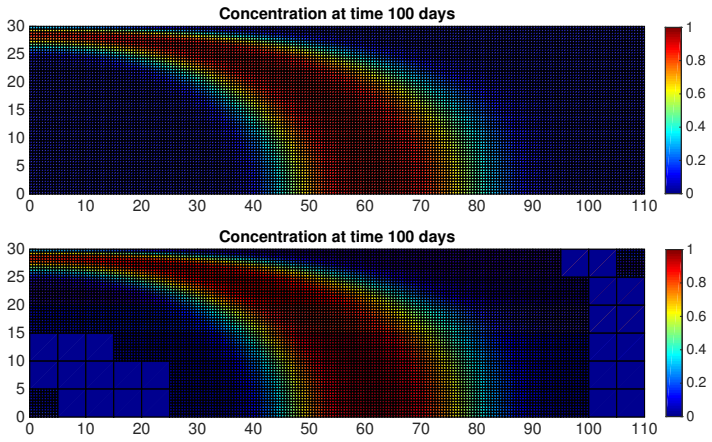

Figure 15: Concentration profiles at 100 days for fine (top) and adaptive (bottom) approaches

Figure 16 shows the tracer concentration history at the production well after 200 days. The fine and adaptive results are in excellent agreement. Since the fine scale permeability distribution is homogeneous the homogenized or coarse scale distribution is also spatially invariant at 50mD. The disagreement between homogenized and fine results can be directly attributed to the numerical diffusion owing to the coarse grid. We also notice that different adaptivity criteria generate the same solution accuracy for the homogeneous permeability distribution indicating that such a criterion is significant a heterogeneous case.

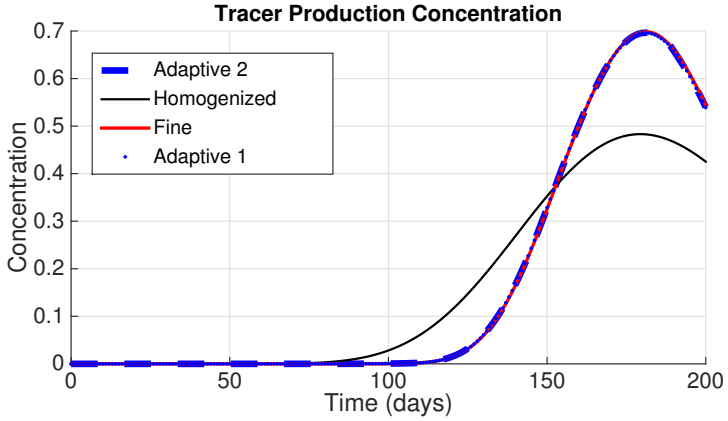

Figure 16: Tracer concentration history at production well for a homogeneous permeability distribution of 50 mD

Gaussian Permeability Distribution

For this numerical test, we choose a layered permeability distribution as shown in Fig. 17 (top) obtained by extracting a slice of SPE10 dataset at layer 20. The coarse scale permeability, Fig. 17 (bottom), distribution is evaluated using the numerical homogenization approach described before.

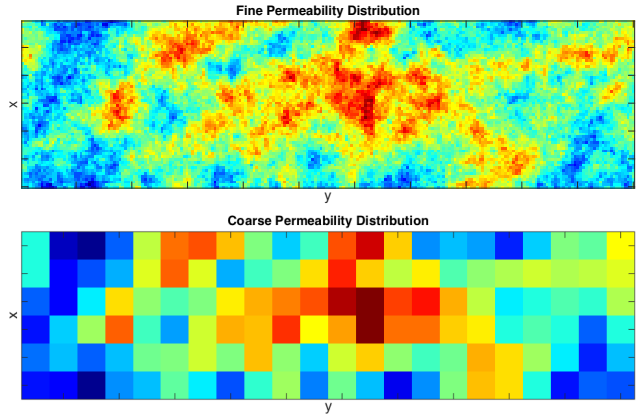

Figure 17: Fine and coarse scale permeability distributions for SPE 10 layer 20

Fig. 18 shows the concentration profiles after 100 days for the coarse scale using homogenization, fine scale, and adaptive homogenization approaches.

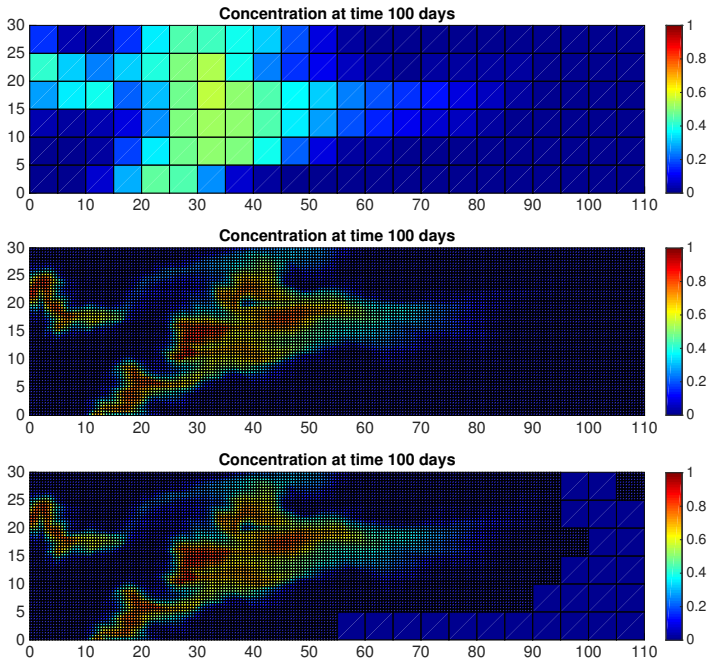

Figure 18: Concentration profiles at 100 days for coarse (top) , fine (middle) and adaptive (bottom) approaches

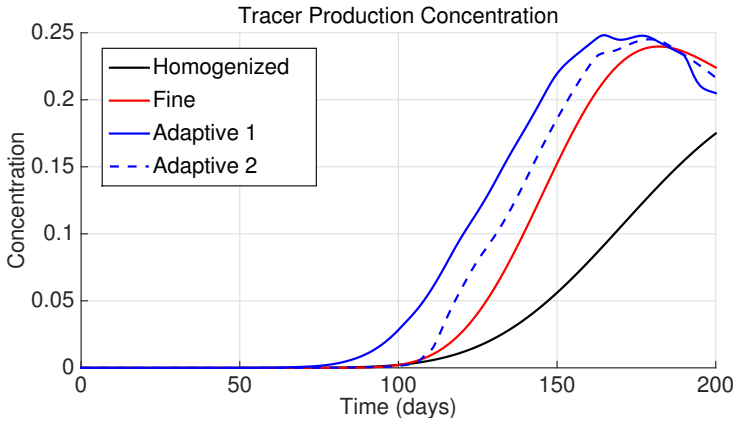

Figure 19: Tracer concentration history at the production well for SPE layer 20.

Figure 19 shows the tracer concentration history at the production well after 200 days. The results show that the concentrations using adaptive homogenization approaches are in good agreement with the fine scale solution. Further, the second adaptivity criteria based upon gradient of concentration at the coarse scale performs better than the first adaptivity criterion relying on temporal change in concentration at the coarse scale.

Channelized Permeability Distribution

Here we choose the permeability distribution from layer 37 of the SPE10 dataset. The coarse scale permeability distribution, Fig. 20 (bottom), distribution is evaluated as in the previous example.

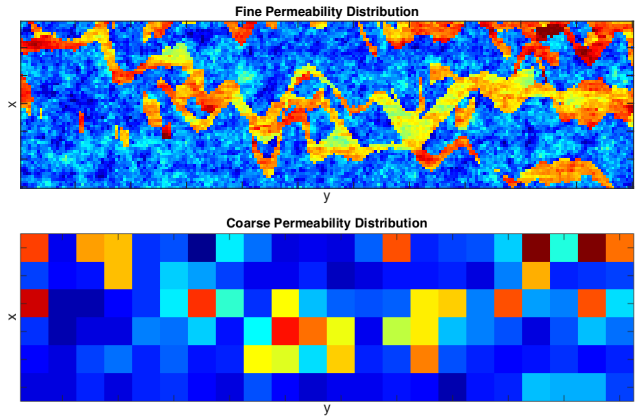

Figure 20: Fine and coarse scale permeability distributions for SPE 10 layer 37

Fig. 21 shows the concentration profiles after 100 days for the coarse scale using homogenization, fine scale, and adaptive homogenization approaches. These results indicated that even for highly channelized permeability distribution adaptive homogenization approach is able to accurately represent the concentration front when compared to the fine scale benchmark solution. The coarse

scale using solely numerical homogenization however smudges the front substantially leading to drastic differences in breakthrough time prediction of the numerical simulation. Thus the adaptive homogenization approach is appropriate for both multimodal or layered permeability distributions in addition to Gaussian permeability distributions.

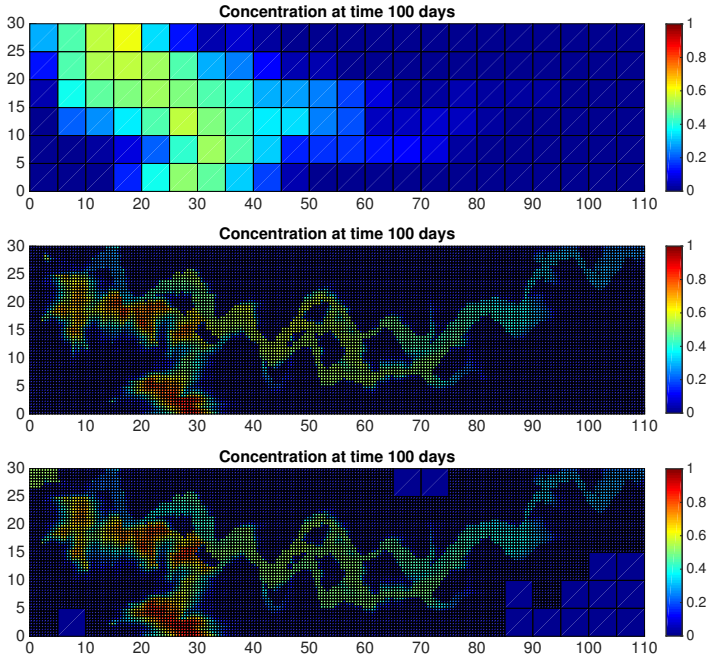

Figure 21: Concentration profiles at 100 days for coarse (top) , fine (middle) and adaptive (bottom) approaches

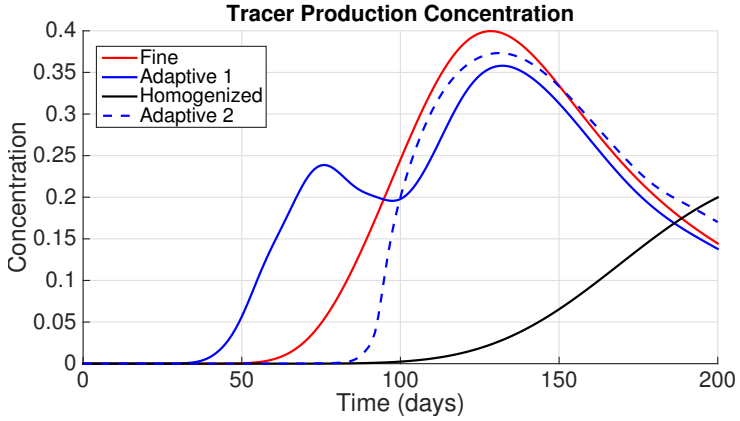

Figure 22: Tracer concentration history at the production well for SPE layer 37.

Figure 22 shows the tracer concentration history at the production well after 200 days. Please

note that the homogenized, or coarse using numerical homogenization only, deviates more drastically from the fine scale solution for the layered permeability distribution (SPE layer 37) compared to the Gaussian permeability distribution (SPE layer 20) as shown in Figure 19. Again, the second adaptivity criterion performs better in capturing the fine scale physics.

6 Conclusions

We developed an adaptive multiscale scheme using local numerical homogenization and EV MFEM for upscaling single phase flow and transport in a heterogeneous porous media. The numerical and adaptive homogenization schemes were numerically verified against a benchmark fine scale solution. The results are in excellent agreement due to an accurate identification of the concentration fronts (transient zones). The numerical results on different layers of SPE10 also indicate that an upscaling based solely upon numerical homogenization is in good agreement with the fine scale solution for a Gaussian or periodic permeability distribution. However, for highly channelized for layered permeability distributions the results deviate substantially. The adaptive multiscale scheme, on the other hand, is in good agreement for Gaussian, periodic, and layered permeability distributions and is approximately $4\times$ faster than the fine scale simulation for a tracer slug injection of 50 days in all the above numerical tests. Please note that a tracer slug injection is specifically chosen to test adaptivity since there are two transient regions at the front and back of the injected slug. The accuracy of the adaptive multiscale approach presented here, compared to the fine scale solution, is dependent on the nature of physical process and validity of the adaptivity criteria in capturing fine scale physics. An optimal tolerance for the adaptivity criteria is chosen to reduce computational cost without substantial loss in solution accuracy.

Acknowledgements

This work was funded by the DOE-NETL grant DE-FE0023314. We are thankful for the opportunity enabling us to conduct this research. We would also like to thank our Center for Subsurface Modeling Industrial affiliates for their continuing support.

References

[1] Jørg E Aarnes and Yalchin Efendiev. An adaptive multiscale method for simulation of fluid flow in heterogeneous porous media. *Multiscale Modeling & Simulation*, 5(3):918–939, 2006.

[2] Assyr Abdulle, E Weinan, Björn Engquist, and Eric Vanden-Eijnden. The heterogeneous multiscale method. *Acta Numerica*, 21:1–87, 2012.

[3] Grégoire Allaire. Homogenization and two-scale convergence. *SIAM Journal on Mathematical Analysis*, 23(6):1482–1518, 1992.

[4] Brahim Amaziane, Alain Bourgeat, and Mladen Jurak. Effective macrodiffusion in solute transport through heterogeneous porous media. *Multiscale Modeling & Simulation*, 5(1):184–204, 2006.

[5] Ilona Ambartsumyan, Eldar Khattatov, Jan Nordbotten, and Ivan Yotov. A multipoint stress mixed finite element method for elasticity I: Simplicial grids. Preprint.

[6] Ilona Ambartsumyan, Eldar Khattatov, Jan Nordbotten, and Ivan Yotov. A multipoint stress mixed finite element method for elasticity II: Quadrilateral grids. Preprint.

[7] Todd Arbogast. Implementation of a locally conservative numerical subgrid upscaling scheme for two-phase darcy flow. *Computational Geosciences*, 6(3-4):453–481, 2002.

[8] Todd Arbogast. *Mixed Multiscale Methods for Heterogeneous Elliptic Problems*, pages 243–283. Springer Berlin Heidelberg, Berlin, Heidelberg, 2012.

[9] Todd Arbogast, Steven L Bryant, et al. Numerical subgrid upscaling for waterflood simulations. In *SPE Reservoir Simulation Symposium*. Society of Petroleum Engineers, 2001.

[10] Todd Arbogast, Susan E Minkoff, and Philip T Keenan. *An operator-based approach to upscaliiig the pressure equation*, volume 23. WIT Press, 1998.

[11] Todd Arbogast, Gergina Pencheva, Mary F Wheeler, and Ivan Yotov. A multiscale mortar mixed finite element method. *Multiscale Modeling & Simulation*, 6(1):319–346, 2007.

[12] Todd Arbogast, Zhen Tao, and Hailong Xiao. Multiscale mortar mixed methods for heterogeneous elliptic problems. *Contemp. Math*, 586:9–21, 2013.

[13] Todd Arbogast and Mary F Wheeler. A nonlinear mixed finite element method for a degenerate parabolic equation arising in flow in porous media. *SIAM Journal on Numerical Analysis*, 33(4):1669–1687, 1996.

[14] Ivo Babuška, Gabriel Caloz, and John E Osborn. Special finite element methods for a class of second order elliptic problems with rough coefficients. *SIAM Journal on Numerical Analysis*, 31(4):945–981, 1994.

[15] Ivo Babuška and John E Osborn. Generalized finite element methods: their performance and their relation to mixed methods. *SIAM Journal on Numerical Analysis*, 20(3):510–536, 1983.

[16] Matthew T Balhoff, Sunil G Thomas, and Mary F Wheeler. Mortar coupling and upscaling of pore-scale models. *Computational Geosciences*, 12(1):15–27, 2008.

[17] Alain Bensoussan, Jacques-Louis Lions, and George Papanicolaou. *Asymptotic analysis for periodic structures*, volume 5. North-Holland Publishing Company Amsterdam, 1978.

[18] Eric Chung, Yalchin Efendiev, and Thomas Y Hou. Adaptive multiscale model reduction with generalized multiscale finite element methods. *Journal of Computational Physics*, 320:69–95, 2016.

[19] Eric T Chung, Yalchin Efendiev, and Wing Tat Leung. Generalized multiscale finite element methods for wave propagation in heterogeneous media. *Multiscale Modeling & Simulation*, 12(4):1691–1721, 2014.

[20] B Fraeijs De Veubeke. Displacement and equilibrium models in the finite element method. *Stress analysis*, 9:145–197, 1965.

[21] Louis J Durlofsky. Upscaling of geocellular models for reservoir flow simulation: A review of recent progress. In *7 th International Forum on Reservoir Simulation*. Citeseer, 2003.

[22] Yalchin Efendiev and Thomas Y Hou. *Multiscale finite element methods: theory and applications*, volume 4. Springer Science & Business Media, 2009.

[23] Björn Engquist, Xiantao Li, Weiqing Ren, Eric Vanden-Eijnden, et al. Heterogeneous multiscale methods: a review. *Communications in Computational Physics*, 2(3):367–450, 2007.

[24] C. L. Farmer. Upscaling: a review. *International Journal for Numerical Methods in Fluids*, 40(1):63–78.

[25] Benjamin Ganis, Kundan Kumar, Gergina Pencheva, Mary F. Wheeler, and Ivan Yotov. A global jacobian method for mortar discretizations of a fully implicit two-phase flow model. *Multiscale Modeling & Simulation*, 12(4):1401–1423, 2014.

[26] Benjamin Ganis and Ivan Yotov. Implementation of a mortar mixed finite element method using a multiscale flux basis. *Computer Methods in Applied Mechanics and Engineering*, 198(49):3989–3998, 2009.

[27] Vivette Girault, Danail Vassilev, and Ivan Yotov. Mortar multiscale finite element methods for stokes–darcy flows. *Numerische Mathematik*, 127(1):93–165, 2014.

[28] Kåre Hellan. Analysis of elastic plates in flexure by a simplified finite element method. *Acta Polytechnica Scandinavica - Civil Engineering and Building Construction Series*, (46):1, 1967.

[29] Thomas Y. Hou and Xiao-Hui Wu. A multiscale finite element method for elliptic problems in composite materials and porous media. *Journal of Computational Physics*, 134(1):169–189.

[30] Susan D Hovorka, Shinichi Sakurai, Yousif K Kharaka, H Seay Nance, Christine Doughty, Sally M Benson, Barry M Freifeld, Robert C Trautz, Tommy Phelps, and Thomas M Daley. Monitoring co2 storage in brine formations: lessons learned from the frio field test one year post injection. *Gulf coast carbon center publication library, Bookshelf*, 2006.

[31] Thomas JR Hughes and Giancarlo Sangalli. Variational multiscale analysis: the fine-scale greens function, projection, optimization, localization, and stabilized methods. *SIAM Journal on Numerical Analysis*, 45(2):539–557, 2007.

[32] Vasilii Vasil'evich Jikov, Sergei M Kozlov, and Olga Arsen'evna Oleinik. *Homogenization of differential operators and integral functionals*. Springer Science & Business Media, 2012.

[33] Andro Mikelić. Homogenization of nonstationary navier-stokes equations in a domain with a grained boundary. *Annali di Matematica pura ed applicata*, 158(1):167–179, 1991.

[34] Andro Mikelić, Vincent Devigne, and CJ Van Duijn. Rigorous upscaling of the reactive flow through a pore, under dominant peclet and damkohler numbers. *SIAM journal on mathematical analysis*, 38(4):1262–1287, 2006.

[35] Grigorios A Pavliotis and Andrew Stuart. *Multiscale methods: averaging and homogenization*. Springer Science & Business Media, 2008.

[36] Gergina V Pencheva, Martin Vohralík, Mary F Wheeler, and Tim Wildey. Robust a posteriori error control and adaptivity for multiscale, multinumerics, and mortar coupling. *SIAM Journal on Numerical Analysis*, 51(1):526–554, 2013.

[37] Thomas F. Russell and Mary Fanett Wheeler. *2. Finite Element and Finite Difference Methods for Continuous Flows in Porous Media*, pages 35–106.

[38] Gurpreet Singh and Mary F. Wheeler. Compositional flow modeling using a multi-point flux mixed finite element method. *Computational Geosciences*, 20(3):421–435, 2016.

[39] Geoffrey Taylor. Dispersion of soluble matter in solvent flowing slowly through a tube. *Proceedings of the Royal Society of London A: Mathematical, Physical and Engineering Sciences*, 219(1137):186–203, 1953.

[40] Sunil G Thomas and Mary F Wheeler. Enhanced velocity mixed finite element methods for modeling coupled flow and transport on non-matching multiblock grids. *Computational Geosciences*, 15(4):605–625, 2011.

[41] Alan Weiser and Mary Fanett Wheeler. On convergence of block-centered finite differences for elliptic problems. *SIAM Journal on Numerical Analysis*, 25(2):351–375, 1988.

[42] John A Wheeler, Mary F Wheeler, and Ivan Yotov. Enhanced velocity mixed finite element methods for flow in multiblock domains. *Computational Geosciences*, 6(3-4).

[43] Stephen Whitaker. Flow in porous media i: A theoretical derivation of darcy's law. *Transport in porous media*, 1(1):3–25, 1986.

[44] Xiao-Hui Wu, Y Efendiev, and Thomas Y Hou. Analysis of upscaling absolute permeability. *Discrete and Continuous Dynamical Systems Series B*, 2(2):185–204, 2002.